J. Fluid Mech. (2002), *vol.* 473, *pp.* 275–294.
DOI: 10.1017/S002211200200246X Printed in the United Kingdom

Axisymmetric acoustic scattering by vortices

By Y. HATTORI[1] AND STEFAN G. LLEWELLYN SMITH[2]

[1]Department of Computer Aided Science, Kyushu Institute of Technology, Tobata, Kitakyushu 804-8550, Japan

[2]Department of Mechanical and Aerospace Engineering, University of California San Diego, 9500 Gilman Drive, La Jolla, CA 92093-0411, USA

(Received 19 October 2001 and in revised form 8 July 2002)

The scattering of acoustic waves by compact three-dimensional axisymmetric vortices is studied using direct numerical simulation in the case where the incoming wave is aligned with the symmetry axis and the direction of propagation of the vortices. The cases of scattering by Hill's spherical vortex and Gaussian vortex rings are examined, and results are compared with predictions obtained by matched asymptotic expansions and the Born approximation. Good agreement is obtained for long waves, with the Born approximation usually giving better predictions, especially as the difference in scale between vortex and incoming waves decreases and as the Mach number of the flow increases. An improved version of the Born approximation which takes into account higher-order effects in Mach number gives the best agreement.

1. Introduction

The generation of sound by fluid flows has been an important area of research since the pioneering work of Lighthill (1952). The scattering of sound by vortices has possibly an even longer history (Obukhov 1941), with applications to the propagation of sound through turbulence (Kraichnan 1953; Lighthill 1953; Batchelor 1956) and through the wakes of engines (the 'aircraft wake problem' mentioned by Ferziger 1974). More recently, Lund & Rojas (1989) proposed using scattering by ultrasound to probe turbulence in laboratory experiments. New non-invasive measurement techniques have since been developed using this idea (Labbé & Pinton 1998; Oljaca *et al.* 1998; Dernoncourt, Pinton & Fauve 1998; Manneville *et al.* 1999).

The problem of the scattering of acoustic waves by simple vortices is neither new nor unexplored (Obukhov 1941; Lindsay 1948; Müller & Matschat 1959; Pitaevskii 1959; Fetter 1964; Georges 1972; Ferziger 1974; O'Shea 1975; Golemshtok & Fabrikant 1980; Kambe & Mya Oo 1981; Tanaka & Ishii 1981; Fabrikant 1983; Howe 1983; Kop'ev & Leont'ev 1987; Reinschke, Möhring & Obermeier 1997). Most of these studies were limited to simple analytical distributions such as point vortices, which were sometimes physically unrealistic; the studies also did not always proceed from a rational set of equations. These studies mostly investigated two limits: one in which the acoustic waves have small wavelength compared with the scale of the vortex – the WKB limit; the other in which the acoustic waves have long wavelength compared with the scale of the vortex – the Born limit. The Born limit uses Lighthill's acoustic analogy, which will be explained later, to obtain a solution.

Ford & Llewellyn Smith (1999) investigated the problem of scattering of a plane sound wave by a two-dimensional vortex using matched asymptotic expansions (MAE) in the Born limit. For small Mach number M, the equations are solved

as an asymptotic expansion in M and δ, the non-dimensional amplitude of the incoming wave. There are then two different regions in the flow: a region centred on the vortex with the length scale of the vortex L, and a wave region where the typical length scale is the acoustic wavelength $\lambda \sim LM^{-1}$. This approach helped resolve the apparent singularity in the forward scatter direction obtained previously (see also Sakov 1993 and Howe 1999). The same ideas have since been used to develop a general formulation for the theoretical solution of the scattering of plane waves by vortices in three dimensions using MAE (Llewellyn Smith & Ford 2001*a*, *b*, hereafter LSF*a*, *b*). These results essentially show that the acoustic analogy predictions are appropriate provided the vortical flow is not evolving rapidly due to instability or incipient singularity formation (should such a scenario prove possible). Howe (1984) discussed the influence of the time-dependence of a body of turbulence on the interaction with an incident sound wave.

Problems of sound generation by flows have also been considered using computer simulations, and this field has become known as computational aeroacoustics. An excellent collection of articles is Hardin & Hussaini (1993). Computational aeroacoustics encompasses a wide span of techniques, from direct numerical simulations (DNS) of compressible flows to solutions of the acoustic analogy with a given flow field. DNS calculations to date have mainly been restricted to two dimensions or to axisymmetric situations (Colonius, Lele & Moin 1994; Mitchell, Lele & Moin 1995, 1999; Tang & Ko 1997; Inoue & Hattori 1999; Grasso & Pirozzoli 2000; Inoue, Hattori & Sasaki 2000).

In this paper, we present results from DNS studies of axisymmetric scattering of plane acoustic waves by Hill's spherical vortex (HSV) and by Gaussian vortex rings, both of which may be viewed as prototypes of propagating three-dimensional vortices. As in the vast majority of previous work, we limit ourselves to small-Mach-number flow. In § 2 we outline the problem, while in § 3 we review previous theoretical work on acoustic scattering by three-dimensional vortices using MAE and the Lighthill acoustic analogy. We present results of the DNS in § 4 where we discuss the dependence on the parameters of the problem, and compare DNS scattering cross-sections to the theoretical predictions outlined earlier. Finally, we conclude in § 5.

2. Statement of the problem

2.1. *Governing equations and flow configuration*

Figure 1 shows a schematic diagram of the flow configuration. A plane incoming wave whose amplitude is small interacts with a vortex. Both viscous effects and the thermal diffusion are assumed to be small; they are neglected in the analysis, while they are small but non-zero in the numerical calculations.

The equations of motion for a homentropic gas are

$$\rho_a \frac{\mathrm{D}\boldsymbol{u}}{\mathrm{D}t} = -\nabla p_a, \tag{2.1a}$$

$$\frac{\mathrm{D}\rho_a}{\mathrm{D}t} + \rho_a \nabla \cdot \boldsymbol{u} = 0, \tag{2.1b}$$

$$\frac{p_a}{p_0} = \left(\frac{\rho_a}{\rho_0}\right)^{\gamma}. \tag{2.1c}$$

Here, $\boldsymbol{u}$ is the velocity, p_a is the absolute pressure, and ρ_a is the absolute density. The relation (2.1*c*) is the equation of state for a homentropic ideal gas, and $\gamma > 1$ is the

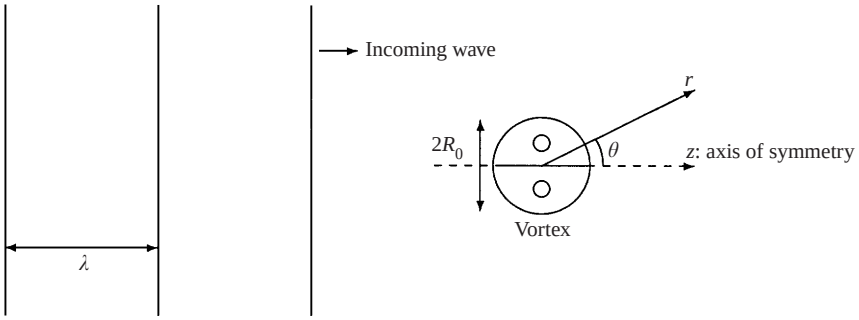

FIGURE 1. Schematic diagram of flow configuration.

constant ratio of specific heats. The constants p_0 and ρ_0 are reference values of the pressure and density respectively, which we shall take to be the uniform values of pressure and density when the fluid is at rest.

The typical flow velocity and the size of the 'vortical region' in which vorticity is concentrated are denoted by U and L, respectively. The Mach number M of the vortex is then defined to be $M \equiv U/c_0 \ll 1$, where $c_0 \equiv (\gamma p_0/\rho_0)^{1/2}$ is the speed of linear sound waves in (2.1). We consider the case where M is small. The velocity scale U and length scale L define a time scale $\tau_v \equiv L/U$ appropriate to flow in the vortical region.

A plane acoustic wave is incident from infinity with wavelength λ, frequency ω_0, and hence wavenumber $k_0 = 2\pi/\lambda$, with $\omega_0 = k_0 c_0$.

2.2. *Hill's vortex*

Hill's spherical vortex (HSV) is the simplest exact axisymmetric solution of the three-dimensional vorticity equations. It has a simple form in a frame in which it is stationary, and there is then a uniform flow $-U\boldsymbol{e}_z$ at infinity. The Stokes streamfunction ψ_0' is then

$$\frac{\psi_0'}{UR_0^2} = \begin{cases} \frac{3}{4}[1-(r/R_0)^2](r/R_0)^2\sin^2\theta, & r/R_0 < 1, \\ -\frac{1}{2}[1-(R_0/r)^3](r/R_0)^2\sin^2\theta, & r/R_0 > 1. \end{cases} \tag{2.2}$$

In this expression, r is the distance from the centre of the vortex, and θ is the usual polar angle. The length scale L is set to be R_0, which is the radius of the vortex.

In a frame in which the medium is at rest at infinity, the streamfunction for the moving HSV becomes

$$\frac{\psi_0}{UR_0^2} = \begin{cases} \frac{1}{4}[5-3(r/R_0)^2](r/R_0)^2\sin^2\theta, & r/R_0 < 1, \\ \frac{1}{2}(R_0/r)\sin^2\theta, & r/R_0 > 1. \end{cases} \tag{2.3}$$

Here r is the distance from the moving centre of the vortex, which has velocity $U\boldsymbol{e}_z$.

LSF*b* calculate the axisymmetric acoustic scattering by HSV explicitly, using the fact that there is a conserved quantity (see the instability analysis of Moffatt & Moore 1978). For the non-axisymmetric case, such an exact solution is no longer possible. (Fukuyu, Ruzi & Kanai 1994 investigated the general non-axisymmetric stability problem numerically.)

2.3. *Gaussian vortex ring*

Although HSV is one of the most important solutions to the Euler equation, it is not close to the vortex rings observed experimentally. Most of the vortex rings observed in experiments have thin cores. Norbury (1973) found a family of vortex rings characterized by the ratio of the core radius and the ring radius, of which HSV is the fattest member. Norbury's vortex rings have vorticity proportional to the distance from the axis of symmetry and the vorticity is discontinuous at the boundary of the vortex core.

In addition to HSV, we deal with a more realistic vortex ring whose vorticity distribution is given by a Gaussian distribution

$$\omega_\varphi(z,\sigma) = \frac{\Gamma}{\pi R_c^2}\exp\left[-\frac{z^2+(\sigma-R_0)^2}{R_c^2}\right], \tag{2.4}$$

where σ is the distance from the axis of symmetry, Γ is the circulation, R_c is the core radius and R_0 is the radius of the ring. As shown by Saffman (1970), for viscous vortex rings the vorticity distribution evolves into the Gaussian distribution at leading order provided that its initial core radius is sufficiently small (for the higher-order corrections, see Fukumoto & Moffatt 2000). Experimentally observed vorticity distributions are often close to the Gaussian distributions (e.g. Sullivan, Widnall & Ezekiel 1973).

3. Theoretical results

3.1. *Acoustic analogy solution and its improved version*

The approach that we call the acoustic analogy here usually proceeds as follows. Following Lighthill (1952), the equations are rewritten as a single inhomogeneous wave equation with all the remaining terms on the right-hand side. The quadrupole source term is usually written $\partial^2 T_{ij}/\partial x_i \partial x_j$, where x_i are Cartesian coordinates and T_{ij} is the Lighthill tensor. For small-Mach-number flows, the tensor is approximated by $T_{ij} \approx \rho_0 u_i u_j$, where ρ_0 is the mean density, and the u_i are velocity components. In turn, the scattered field is then computed by expanding

$$T_{ij} \approx \rho_0 v_i v_j + \rho_0(u_i^L v_j + v_i u_j^L) + \rho_0 u_i^L u_j^L, \tag{3.1}$$

where u_i^L and v_i are the velocities due to the acoustic wave and the vortex flow respectively (see Kambe & Mya Oo 1981).

There is no *a priori* reason why this approximation to T_{ij} should yield the correct scattered sound, because the velocity field in the vicinity of the vortex is most definitely not the superposition of wave and vortex. Nevertheless, the analysis of LSF*a* shows that in general the acoustic analogy agrees with a rational MAE analysis in the limit of large wavelength.

In fact, the first term in (3.1) does not contribute to the scattered sound field, since it is steady. The last is usually neglected, and corresponds to wave–wave interaction. The velocity scaling of the incoming wave in the inner region is given by ac_0, where $a \equiv |p_i|/\rho_0 c_0^2$ is the non-dimensionalized amplitude of the incoming wave. Note that a is related to $\delta \equiv |p_i|/\rho_0 U^2$, which is the non-dimensionalized amplitude used in LSF*a*, by $a = \delta M^2$. Thus, evaluating the size of the three different terms gives $\rho_0 M^2 c_0^2$ (irrelevant), $\rho_0 a M c_0^2$ and $\rho_0 a^2 c_0^2$, which justifies our neglect of the wave–wave term since $a \ll M$ is normally satisfied as a is very small. (In our simulations, $a \leqslant O(10^{-5}$–$10^{-4})$.) We shall later consider the first correction to the usual acoustic

analogy solution including the neglected terms in (3.1). This comes from a term $\rho^L v_i v_j$ where ρ^L is the density disturbance associated with the incoming acoustic wave. The scaling for ρ^L is $\rho_0 a$, so the size of the correction term is $\rho_0 a M^2 c_0^2$, i.e. a factor of M smaller than the dominant term.

The acoustic analogy solution of Kambe & May Oo (1981) is

$$p(r,\theta,t) = \frac{|p_i|}{r} f_1(\theta) \mathrm{e}^{\mathrm{i}\omega_s(t-r/c_0)}, \tag{3.2}$$

$$f_1(\theta) = -\frac{\omega_s^2}{2\pi(1-M_v\cos\theta)c_0^3} V_n(\boldsymbol{\kappa}_0)\cos\theta, \tag{3.3}$$

where M_v is the Mach number based on the speed of vortex, $V_n(\boldsymbol{\kappa})$ is the Fourier transform of the velocity component $\boldsymbol{u}\cdot\boldsymbol{n}$ and

$$\boldsymbol{\kappa}_0 = (1-\beta)k_0\boldsymbol{n} - k_0\boldsymbol{i},$$

$$\beta = M_v(1-\cos\theta)/(1-M_v\cos\theta),$$

$$\omega_s = (1-\beta)\omega_0,$$

where $\boldsymbol{n}$ and $\boldsymbol{i}$ are the unit vectors in the directions of θ and the incoming wave, respectively.

The above scattered wave includes the Doppler factor $1-M_v\cos\theta$ which is replaced by unity for sufficiently small M_v. In other words the amplitude factor (3.3) includes not only the leading-order term $O(M)$ but also the next-order term $O(M^2)$. The equation (3.3), however, is not sufficient as an approximation up to $O(M^2)$. The exact Lighthill tensor for inviscid flow can be written as

$$T_{ij} = (\rho^V + \rho^L)(v_i + u_i^L)(v_j + u_j^L) + (p^L - c_0^2\rho^L)\delta_{ij} \tag{3.4}$$

$$= \rho^V v_i v_j + \rho^V(u_i^L v_j + v_i u_j^L) + \rho^L v_i v_j + \rho^L(c^2 - c_0^2)\delta_{ij} + O(\rho_0 a M^3 c_0^2, \rho_0 a^2 c_0^2), \tag{3.5}$$

where $\rho = \rho^V + \rho^L$, $p = p^V + p^L$, $c^2 = \gamma p^V/\rho^V$ and the superscript ^{V} denotes the steady field due to the vortex. The terms $\rho^L v_i v_j$ and $\rho^L(c^2 - c_0^2)\delta_{ij}$ give $O(M^2)$ contributions. These terms lead to the following scattering amplitude factors if we replace ρ^L by the incoming wave:

$$f_2(\boldsymbol{n}) = -\frac{\omega_s^2}{4\pi c_0^4}\frac{1}{1-M_v\cos\theta} n_i n_j \tilde{B}_{ij}(\boldsymbol{\kappa}_0), \tag{3.6}$$

$$f_3(\boldsymbol{n}) = -\frac{\omega_s^2}{4\pi c_0^4}\frac{1}{1-M_v\cos\theta} \tilde{C}(\boldsymbol{\kappa}_0), \tag{3.7}$$

where $\tilde{B}_{ij}(\boldsymbol{\kappa})$ and $\tilde{C}(\boldsymbol{\kappa})$ are the Fourier transforms of $u_i u_j$ and $c^2 - c_0^2$, respectively. We call the sum of equations (3.3), (3.6) and (3.7) the improved Born approximation. Appendix A details the derivation of scattering amplitudes (3.6) and (3.7).

3.2. *MAE solution*

The MAE approach of LSF*a* begins by non-dimensionalizing the equations of motion in the vortical and wave region. In the vortex region, the variables are non-dimensionalized by ρ_0, U, L; that is,

$$t^* \equiv \frac{Lt}{U}, \quad \boldsymbol{x}^* \equiv \frac{\boldsymbol{x}}{L}, \quad \rho_a^* \equiv \frac{\rho_a}{\rho_0}, \quad \boldsymbol{u}^* \equiv \frac{\boldsymbol{u}}{U}, \quad p_a^* \equiv \frac{p_a}{\rho_0 U^2}.$$

We further set

$$p_a^* = p_0^*(1+\gamma M^2 p), \quad \rho_a^* = 1 + M^2\rho, \tag{3.8}$$

where $p_0^* \equiv p_0/\rho_0 U^2 = 1/\gamma M^2$, since pressure and density depart from their uniform background values by $O(M^2)$, consistent with near-incompressible motion (Crow 1970). Then the equations of motion become

$$(1+M^2\rho)\frac{\mathrm{D}\boldsymbol{u}^*}{\mathrm{D}t^*} = -\nabla p, \tag{3.9a}$$

$$M^2\left(\frac{\mathrm{D}\rho}{\mathrm{D}t^*} + \rho\nabla\cdot\boldsymbol{u}^*\right) + \nabla\cdot\boldsymbol{u}^* = 0, \tag{3.9b}$$

$$1+\gamma M^2 p = (1+M^2\rho)^\gamma. \tag{3.9c}$$

In the wave region, as the appropriate length scale and time scale are $M^{-1}L$ and $M^{-1}L/c_0 = L/U$, the variables are non-dimensionalized by ρ_0, c_0, $M^{-1}L$; that is,

$$T^* \equiv \frac{Lt}{Mc_0}(= t^*), \quad \boldsymbol{X}^* \equiv \frac{M\boldsymbol{x}}{L}, \quad H_a^* \equiv \frac{\rho_a}{\rho_0}, \quad \boldsymbol{U}^* \equiv \frac{\boldsymbol{u}}{c_0}, \quad P_a^* \equiv \frac{p_a}{\rho_0 c_0^2}.$$

As in the vortical region, we set

$$P_a^* = P_0^*(1+\gamma M^2 P), \quad H_a^* = 1 + M^2 H, \tag{3.10}$$

where $P_0^* = 1/\gamma$. In addition the velocity is scaled as

$$\boldsymbol{U}^* = M^2\boldsymbol{U}. \tag{3.11}$$

Then the equations become

$$(1+M^2H)\left(\frac{\partial\boldsymbol{U}}{\partial T^*} + M^2\boldsymbol{U}\cdot\nabla\boldsymbol{U}\right) = -\nabla P, \tag{3.12a}$$

$$\frac{\partial H}{\partial T^*} + \nabla\cdot\boldsymbol{U} + M^2\nabla\cdot(\boldsymbol{U}H) = 0, \tag{3.12b}$$

$$1+\gamma M^2 P = (1+M^2H)^\gamma, \tag{3.12c}$$

where the gradient operator acting on a wave-region quantity corresponds to differentiation with respect to $\boldsymbol{X}^*$.

To allow for motion of the vortex, the spatial coordinate $\boldsymbol{\xi}$ is defined such that

$$\boldsymbol{\xi} = \boldsymbol{x}^* - \boldsymbol{x}_c^*(t^*), \tag{3.13}$$

where $\boldsymbol{x}_c^*$ is the centre of the vortical region. This definition of the centre is somewhat arbitrary and in fact all that matters is that $\boldsymbol{x}_c^*$ move with the vortex (LSFa).

The incoming wave wavenumber k is non-dimensionalized using the wave-region length scale as $K^* = LM^{-1}k$. Then the final result of LSFa is that the pressure is given at $O(\delta M^4) = O(aM^2)$ in the far field by

$$P_{41} = \frac{1}{4\pi}\mathrm{e}^{-\mathrm{i}\omega_0^* t^*}\left\{\mathrm{e}^{\mathrm{i}K^*X_c^*}\frac{\partial}{\partial\boldsymbol{\Xi}}\left[\left(\boldsymbol{I}^*\cdot\nabla + \mathrm{i}\omega_0^* I_1^*\right)\frac{\mathrm{e}^{\mathrm{i}K^*R^*}}{R^*}\right]\right.$$
$$\left. + \mathrm{e}^{\mathrm{i}K^*X^*}\left(\frac{\partial}{\partial\boldsymbol{\Xi}} - \mathrm{i}\omega_0^*\right)\boldsymbol{I}^*\cdot\nabla\frac{1}{R^*}\right\}, \tag{3.14}$$

where $\boldsymbol{\Xi}$ is the wave-region counterpart of $\boldsymbol{\xi}$. The vector $\boldsymbol{I}^*$ is the vortex centroid of

the flow (Saffman 1992), defined by

$$\boldsymbol{I} \equiv \frac{1}{2}\int \boldsymbol{x}\times\boldsymbol{\omega}(\boldsymbol{x})\,\mathrm{d}^3\boldsymbol{x} \equiv L^3 U \boldsymbol{I}^*. \tag{3.15}$$

The vortex centroid is conserved in incompressible flow, and is hence conserved to $O(M^2)$.

In the far-field limit $R^* \to \infty$, the second of the two terms in (3.14) is $O(R^{*-2})$. The first term contains the radiating waves, and in the limit $R^* \to \infty$ we have

$$P_{41} = -\frac{\omega_0^{*2}}{4\pi}\cos\vartheta\left(\frac{\boldsymbol{I}^*\cdot\boldsymbol{\Xi}}{R^*} + I_1^*\right)\frac{\mathrm{e}^{\mathrm{i}(K^*R^*+K^*X_c^*-\omega_0^*t^*)}}{R^*} + O(R^{*-2}) \tag{3.16}$$

$$= -\frac{\omega_0^{*2}I^*}{4\pi}\cos\vartheta(\cos\vartheta+\cos\mu)\frac{\mathrm{e}^{\mathrm{i}(K^*R^*+K^*X_c^*-\omega_0^*t^*)}}{R^*} + O(R^{*-2}), \tag{3.17}$$

where here ϑ is the angle subtended at the vortex between the position $\boldsymbol{X}^*$ and the direction of propagation of the incident acoustic wave, and μ is the angle between the direction of $\boldsymbol{I}$ and the direction of the propagation of the incident acoustic wave. In dimensional form, the above result becomes

$$p_s = -\frac{|p_i|}{c_0^3}\frac{\omega_0^2 I}{4\pi}\cos\vartheta(\cos\vartheta+\cos\mu)\frac{\mathrm{e}^{\mathrm{i}(kr+kx_c-\omega_0 t)}}{r} + O(r^{-2}). \tag{3.18}$$

This result can be shown to agree with the scattered sound field obtained using the acoustic analogy approximation. Equation (17) of Lund & Rojas (1989) agrees with (3.16), provided that in the former the Fourier transform of the vorticity is approximated as

$$\int \boldsymbol{\omega}(\boldsymbol{x})\,\mathrm{e}^{\mathrm{i}\boldsymbol{k}\cdot\boldsymbol{x}}\,\mathrm{d}^3\boldsymbol{x} \approx \int \mathrm{i}(\boldsymbol{k}\cdot\boldsymbol{x})\boldsymbol{\omega}(\boldsymbol{x})\,\mathrm{d}^3\boldsymbol{x}. \tag{3.19}$$

This approximation is valid provided the length scale of the vortical region is small compared to the wavelength of the incident acoustic waves, which is precisely the condition required for our analysis to be valid. The applicability of the acoustic analogy approximation to vortices with length scale comparable with the wavelength of the incident waves is an open question, which cannot be addressed by the asymptotic analysis presented here.

4. Numerical computations

4.1. *Numerical method*

The numerical method is similar to that used by Inoue *et al.* (2000). The axisymmetric compressible Navier–Stokes equations are solved using a finite-difference method. In order to resolve small-amplitude acoustic waves, the sixth-order compact scheme of Lele (1992) is used for spatial derivatives and a fourth-order Runge–Kutta scheme is used to integrate the solution in time. The non-reflecting boundary conditions of Poinsot & Lele (1992) are used at the boundaries of the numerical domain. In these non-reflecting boundary conditions small deviations in the far field are decomposed into characteristic waves, whose amplitudes A_i are either specified or evolve in time, depending on whether they are incoming or outgoing. Taking the one-dimensional

Euler equations for simplicity, this corresponds to

$$A_i = 0 \text{ for incoming waves,}$$

$$\frac{\partial A_i}{\partial t} + \lambda_i \frac{\partial A_i}{\partial z} = 0 \text{ for outgoing waves,}$$

where the λ_i are the speeds of the characteristic waves. For subsonic flow, $A_1 = p' - \rho_0 c_0 u'$ with $\lambda_1 = u - c_0$ corresponds to the incoming acoustic wave. Thus the boundary conditions can also be used to inject a wave into the domain by specifying the amplitude of the incoming acoustic wave as $A_1 = p_i$ (Colonius *et al.* 1994). Non-uniform grids are used, with the grid spacing set small enough to resolve both vortex and acoustic waves.

The largest grid spacing is 0.05λ, while the grid spacing around the vortices is $0.05R_0$ for HSV and $0.02R_0 = 0.067R_c$ for the Gaussian vortex ring. The grids are stretched gradually through the domain with an increment of less than 4% per grid point. It is known that instability arises for non-uniform grids with these schemes. To remove this instability, we use a pentadiagonal compact filtering scheme (Lele 1992) which is optimized to damp short waves but not to affect acoustic waves.

For each set of parameters three calculations are carried out to obtain the scattered wave: (i) solving for the vortex only (the corresponding pressure field is denoted by p_v); (ii) solving for the incoming wave only (p_i); (iii) solving for the full vortex and incoming wave (p_t). The acoustic signal is obtained from $p_a = p_t - p_v$: this subtraction removes the pressure field due to the vortex and the initial transient waves which are discussed in Appendix B. The scattered wave is then obtained by $p_s = p_a - p_i$. All calculations are carried out in the frame moving with the vortex. The speed of the frame, U_f, however, is 7% to 8% lower than the initial speed of the vortex since the speed of the vortex decreases gradually owing to dissipation.

Initial conditions are characterized as follows. The velocity field is either that of HSV or that of a Gaussian vortex ring. For HSV, we use its compressible extension (LSF*b*), which includes an $O(M^2)$ correction to the original HSV. The pressure and the density are obtained from the condition of uniform entropy and the Poisson equation

$$\nabla^2 \left(\frac{p}{\rho} + \frac{\gamma - 1}{2\gamma} |\boldsymbol{u}|^2 \right) = -\frac{\gamma - 1}{\gamma} \nabla \cdot (\boldsymbol{\omega} \times \boldsymbol{u}). \tag{4.1}$$

For HSV, the Mach numbers based on the vortex speed are $M_v = \pm 0.05, \pm 0.15, \pm 0.3$, where positive and negative M_v correspond to vortices moving in the $+z$-direction and $-z$-direction, respectively. Note that the incoming wave propagates in the $+z$-direction. The Reynolds number based on the speed of sound at infinity is $Re_a = \rho_0 c_0 R_0 / \mu_0 = 25\,000$. For the incoming wave, we consider not only long waves but also waves whose wavelength is comparable to the size of vortex. The wavelength of the incoming wave is set to $\lambda / R_0 = 2, 5, 10$, and its amplitude is set to $|p_i| / \rho_0 c_0^2 = 10^{-5}$. The pressure is observed at $r / R_0 = 10, 20, 30$ in the moving frame. The domain of calculation is $0 \leqslant |x|, \sigma \leqslant 50R_0$. For a Gaussian vortex ring the core radius is fixed at $R_c = 0.3R_0$.

4.2. *Scattering by HSV*

Figure 2 shows an example of the scattered wave as a function of time. The incoming wave, which is injected at the boundary $x = -50R_0$, starts to interact with the vortex at around $t = 50R_0 / (c_0 - U_f)$. Then the scattered wave starts to propagate spherically. The undershoot and the overshoot of the scattered wave in the first period are due

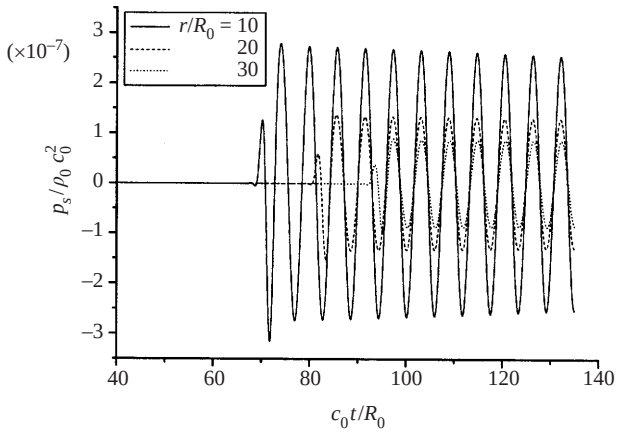

FIGURE 2. Evolution of scattered wave pressure p_s for $M_v = 0.15$ and $\lambda/R_0 = 5$. The observation points are at $r/R_0 = 10$, 20 and 30, and $\theta = 0°$.

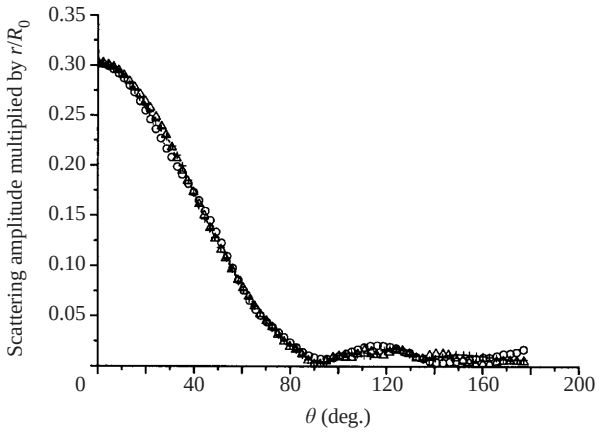

FIGURE 3. Scattering amplitude multiplied by r/R_0 for $M_v = 0.15$ and $\lambda/R_0 = 5$. ○, $r/R_0 = 10$; △, $r/R_0 = 20$; +, $r/R_0 = 30$.

to smoothing of the incoming wave; the incoming wave is filtered according to

$$p_{\text{in}}(t) = |p_i| F(t) \sin(\omega_0' t), \quad F(t) = \begin{cases} \frac{1}{2}[1 - \cos(\omega_0' t)] & \text{for} \quad 0 \leqslant c_0 t/R_0 \leqslant \pi/\omega_0', \\ 1 & \text{for} \quad c_0 t/R_0 \geqslant \pi/\omega_0', \end{cases} \tag{4.2}$$

in order to avoid a discontinuity, where $\omega_0' = \omega_0(1 - U_f/c_0)$ (note that the boundary also moves with the frame). After the first period, the amplitude of the scattered wave is almost constant but decays slightly. The r.m.s. scattering amplitude $\overline{p_s}/\overline{p_i}$ is calculated by averaging over a multiple of the period of the scattered wave at each observation point. Figure 3 shows the scattering amplitude multiplied by r/R_0 against θ for the same case. The three lines corresponding to $r/R_0 = 10$, 20, 30 collapse, which confirms that the scattered wave is a linear spherical wave. Hereafter we use the data at $r/R_0 = 20$.

Figure 4 shows the scattering amplitudes for the large-wavelength case $\lambda = 10R_0$ observed at $r/R_0 = 20$. For $|M_v| = 0.05$, all three predictions are in good agreement with DNS. For $|M_v| = 0.15$, 0.3 MAE does not give a good prediction. The Born

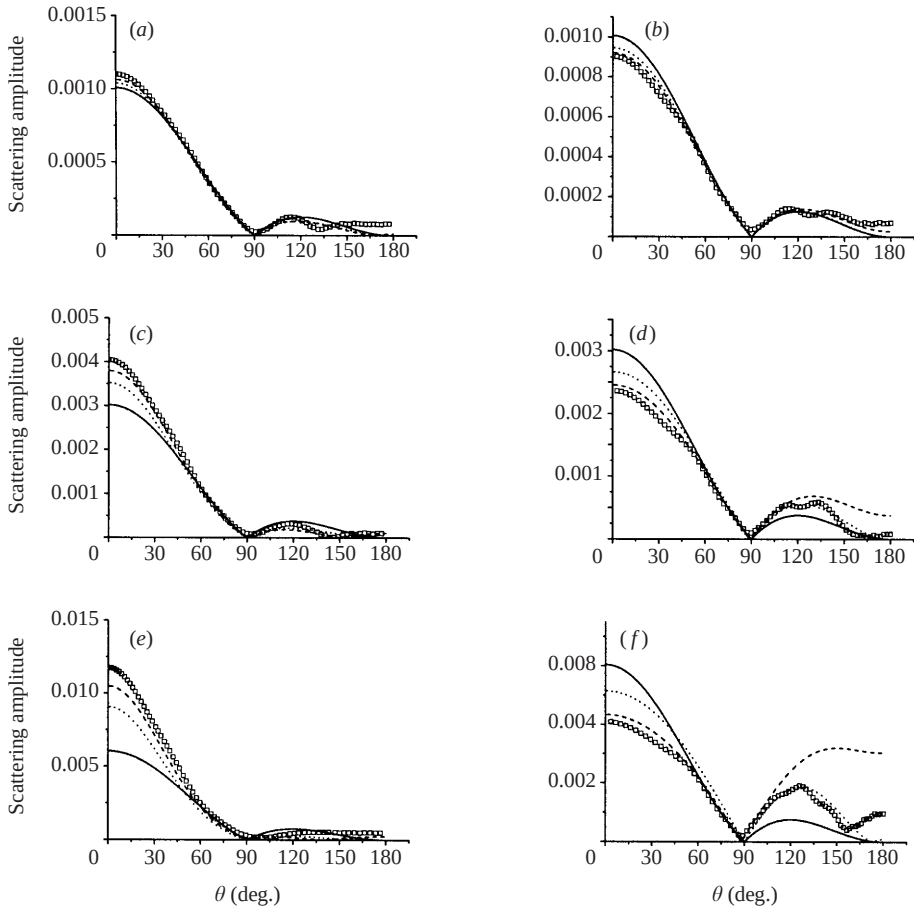

FIGURE 4. Scattering amplitudes. $\lambda/R_0 = 10$, $r/R_0 = 20$. (*a*) $M_v = 0.05$, (*b*) $M_v = -0.05$, (*c*) $M_v = 0.15$, (*d*) $M_v = -0.15$, (*e*) $M_v = 0.3$, (*f*) $M_v = -0.3$. □, DNS results; ——, predictions by MAE; ……, predictions by the Born approximation of Kambe & Mya Oo (1981); – – – –, predictions by the present, improved, Born approximation.

approximation solution of Kambe & Mya Oo (1981) gives a better prediction in the whole range, but the difference with DNS is about 20% around $\theta = 0°$ for $|M_v| = 0.3$. The present improved Born approximation gives the best prediction for $\theta < 90°$; it overpredicts around $\theta = 180°$. We have no satisfactory explanation for this phenomenon at present. MAE gives the same prediction for positive and negative Mach numbers. Thus the difference between DNS and MAE is mainly due to the Doppler effect and the quadrupole term.

Figure 5 shows the scattering amplitudes for $\lambda = 5R_0$. The results are quite similar to those for $\lambda = 10R_0$. All three predictions agree well with DNS for $|M_v| = 0.05$. The difference between MAE and DNS is quite large for $|M_v| = 0.15$ and 0.3, and the improved Born approximation gives the best prediction. The DNS and Born approximations give smaller values in the range $\theta \geqslant 90°$ for $\lambda = 5R_0$ than for $\lambda = 10R_0$.

Figure 6 shows the scattering amplitudes for the shortest wavenumber $\lambda = 2R_0$. The scattering amplitude almost vanishes in the range $\theta \geqslant 90°$, as predicted by the Born approximations. For the lowest Mach number $|M_v| = 0.05$ studied in this paper,

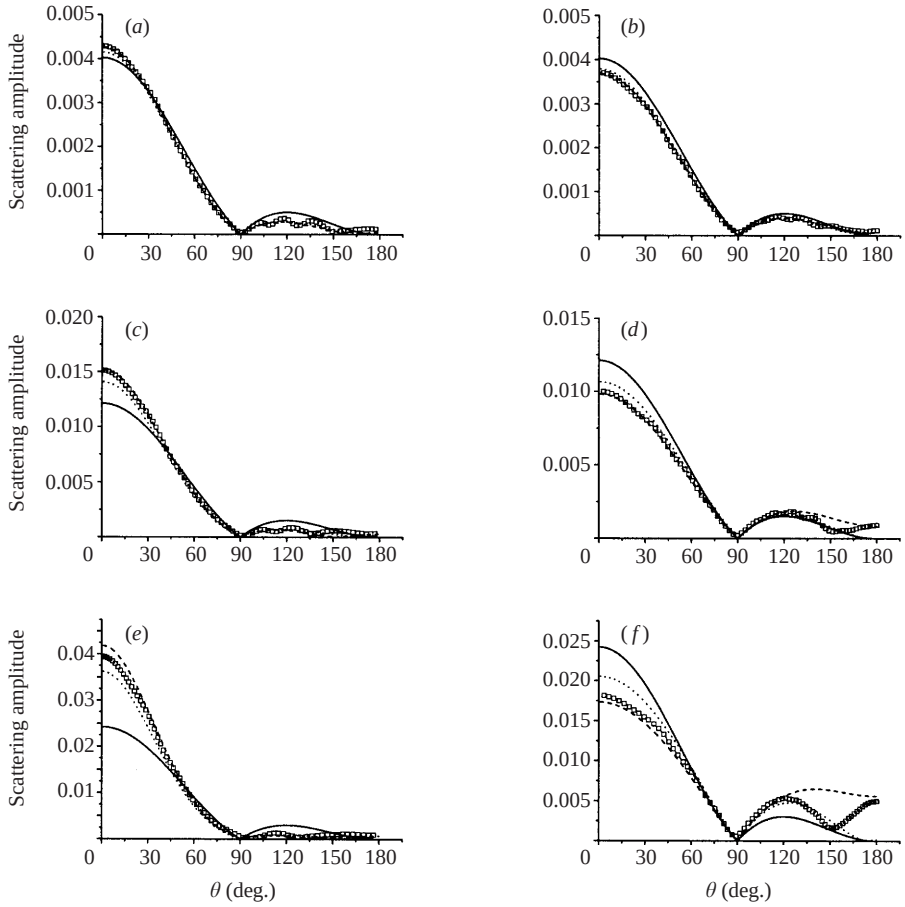

FIGURE 5. Scattering amplitudes. $\lambda/R_0 = 5, r/R_0 = 20$. (*a*) $M_v = 0.05$, (*b*) $M_v = -0.05$, (*c*) $M_v = 0.15$, (*d*) $M_v = -0.15$, (*e*) $M_v = 0.3$, (*f*) $M_v = -0.3$. Symbols and lines as in figure 4.

we see reasonable agreement between DNS and Born approximations. The MAE solution, which assumes long incoming waves, fails to predict the correct directivity of the scattering amplitude. For $|M_v| = 0.15$ and 0.3, however, MAE gives rather good values for the scattering amplitude around $\theta = 0°$. On the other hand, the Born approximations overpredict the scattering amplitude for $M_v > 0$ and underpredict it for $M_v < 0$. This is probably because the scattering amplitude is so large that the Born approximation, in which the total acoustic wave should not differ much from the incoming wave, breaks down. It is worth noting that the scattering amplitude for $M_v > 0$ is smaller than that for $M_v < 0$. For longer wavenumbers $\lambda = 5R_0, 10R_0$, the scattering amplitude for $M_v > 0$ around $\theta = 0°$ is larger than that for $M_v < 0$ by $O(M)$ because of the Doppler factor.

4.3. *Scattering by a Gaussian vortex ring*

Figures 7 and 8 shows the r.m.s. scattering amplitudes for the Gaussian vortex ring. Although the vorticity distribution is quite different from that of HSV, the results are similar to those of HSV. For the shorter wavelength $\lambda/R_0 = 2$, the scattered wave is restricted to a slightly narrower region for the Gaussian vortex ring than for HSV of the same Mach number as shown in figure 9. This is also predicted by the Born

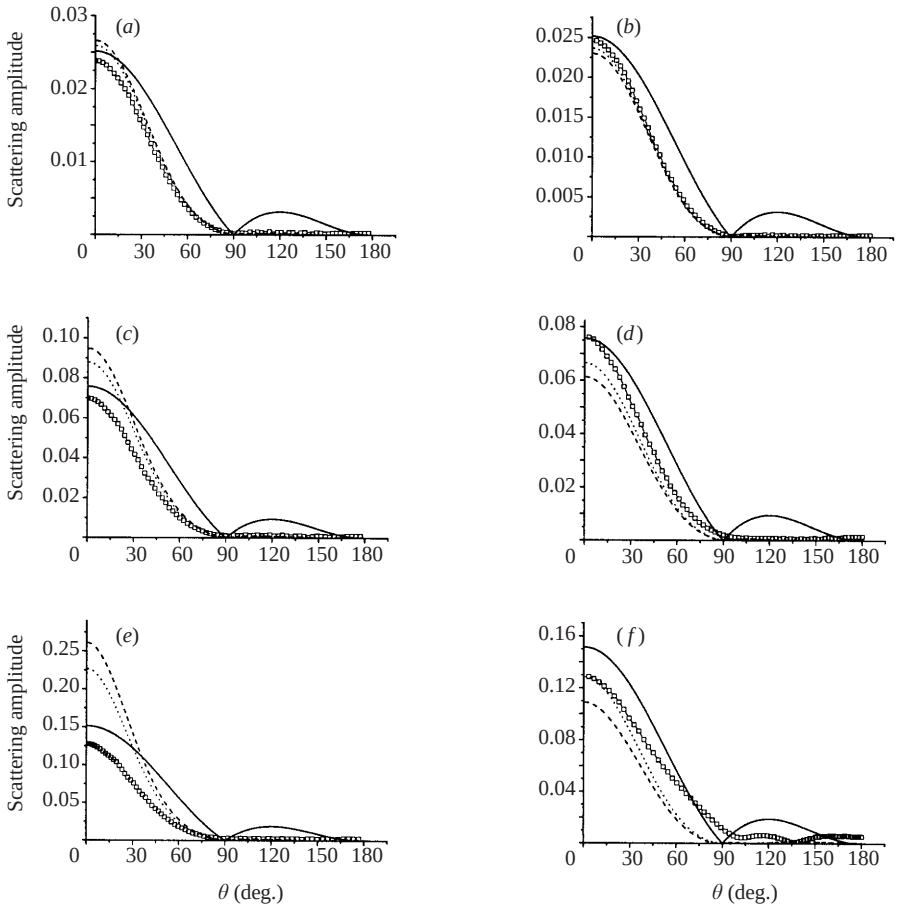

FIGURE 6. Scattering amplitudes. $\lambda/R_0 = 2$, $r/R_0 = 20$. (*a*) $M_v = 0.05$, (*b*) $M_v = -0.05$, (*c*) $M_v = 0.15$, (*d*) $M_v = -0.15$, (*e*) $M_v = 0.3$, (*f*) $M_v = -0.3$. Symbols and lines as in figure 4.

approximations, but they do not give correct magnitudes of the scattering waves for this case.

4.4. *The validity of the Born approximations*

It is of some interest to check the assumption required for the Born approximations *a posteriori*. Figure 10 shows contours of instantaneous pressure for the scattered wave p_s for HSV with $M_v = 0.15$ and $\lambda/R_0 = 10$. In the whole region (figure 10*a*) the scattered waves propagate spherically. In the neighbourhood of HSV (figure 10*b*), where the word 'scattered wave' is not appropriate for p_s, the distribution of p_s is affected by the steady pressure distribution around the vortex. The value of p_s is larger inside the vortex than outside. We are interested in the magnitude of p_s since the Born approximations assume that p_s is small. Figure 11 shows the spatial maximum of p_s as a function of time. It oscillates with a period which is close to one half of the period of the incoming wave in moving coordinates. Its magnitude is less than $0.15|p_i|$. Thus in this case it is reasonable that the Born approximations give good predictions for the scattering amplitudes. For HSV with $M_v = 0.3$ and $\lambda/R_0 = 2$, however, the spatial maximum of p_s oscillates around $1.2|p_i|$. For this case we cannot expect agreement between DNS and the Born approximations as seen in figure 6(*e*).

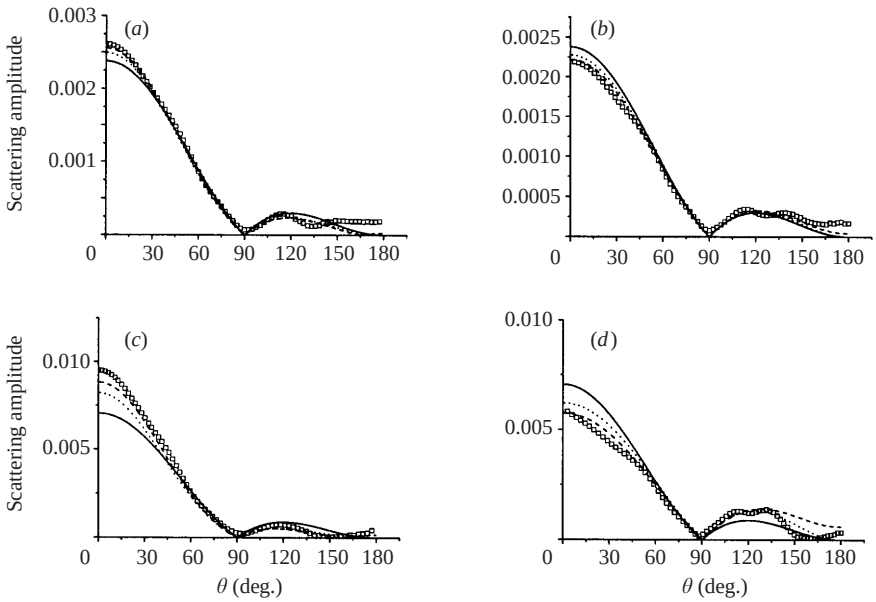

FIGURE 7. Scattering amplitudes. Gaussian vortex ring. $\lambda/R_0 = 10$, $r/R_0 = 20$. (*a*) $M_v = 0.05$, (*b*) $M_v = -0.05$, (*c*) $M_v = 0.15$, (*d*) $M_v = -0.15$. Symbols and lines as in figure 4.

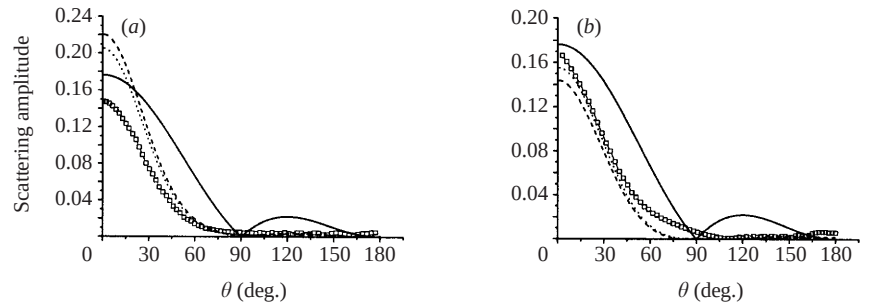

FIGURE 8. Scattering amplitudes. Gaussian vortex ring. $\lambda/R_0 = 2$, $r/R_0 = 20$. (*a*) $M_v = 0.15$, (*b*) $M_v = -0.15$. Symbols and lines as in figure 4.

It is also of interest to check the difference between the Born approximation by Kambe & Mya Oo (1981) and the improved one. Figure 12 compares four lines corresponding to f_1, f_1+f_2, f_1+f_3 and $f_1+f_2+f_3$ (the improved Born approximation). For $\theta < 90°$, the compressibility effect f_3 is small compared to f_1 and f_2. For $\theta > 90°$, f_3 is comparable to f_2. As seen in figures 4 and 5, the improved Born approximation agrees quite well with DNS for $\theta < 90°$ but not for $\theta > 90°$. Thus including the quadrupole effect f_2 is crucial to the improvement of the Born approximation.

4.5. *Total scattering cross-section*

The total scattering cross-section is calculated from

$$\Sigma = 2\pi \int_0^{\pi} \frac{\overline{p_s^2}}{\overline{p_i^2}} r^2 \sin\theta \, \mathrm{d}\theta \tag{4.3}$$

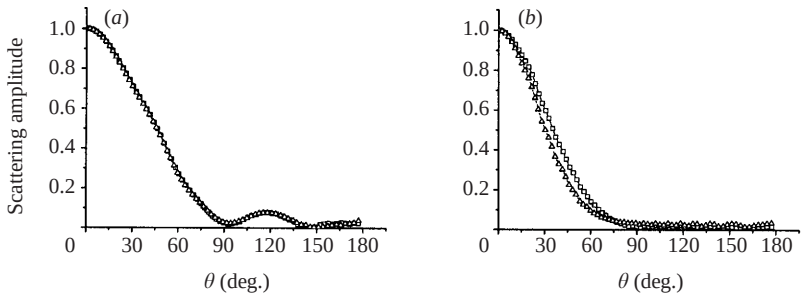

FIGURE 9. Comparison of scattering amplitudes normalized by the maximum values. The squares and triangles correspond to HSV and Gaussian vortex rings, respectively. $M_v = 0.15$, $r/R_0 = 20$. (*a*) $\lambda/R_0 = 10$, (*b*) $\lambda/R_0 = 2$.

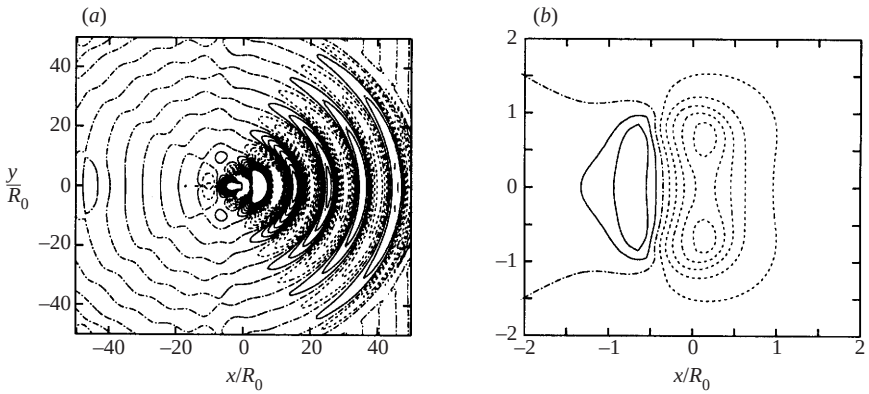

FIGURE 10. Contour lines of p_s for HSV. $c_0 t/R_0 = 120$. Solid lines, dot-dashed lines and broken lines correspond to positive values, zero and negative values, respectively. (*a*) Whole region, max. $= -$min. $= 4 \times 10^{-3}|p_i|$, $\Delta p_s = 5 \times 10^{-4}|p_i|$, (*b*) neighbourhood of HSV, max. $= 4 \times 10^{-2}|p_i|$, min. $= -1 \times 10^{-1}|p_i|$, $\Delta p_s = 2 \times 10^{-2}|p_i|$.

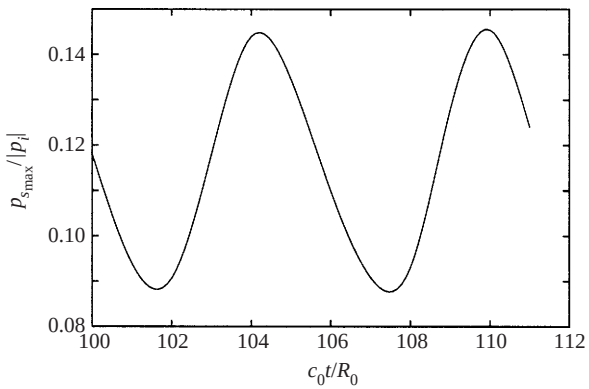

FIGURE 11. Maximum values of p_s for HSV with $M_v = 0.15$, $\lambda/R_0 = 10$.

for the present axisymmetric case. Figure 13 shows the total scattering cross-section for HSV. Note that the MAE values scale as

$$\Sigma \propto M_v^2 \omega_0^4 \propto M_v^2 \lambda^{-4}. \tag{4.4}$$

The agreement in the scattering cross-section between DNS and the three predictions is consistent with that for scattering amplitude: there is good agreement between

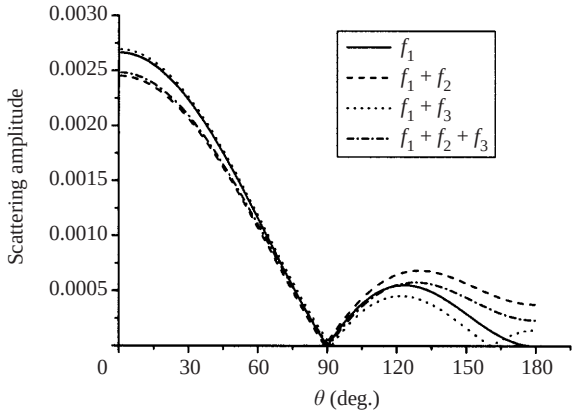

FIGURE 12. The Born approximations for HSV. $M_v = 0.15$, $\lambda/R_0 = 10$. The different line styles correspond to f_1 (Kambe & Mya Oo), $f_1 + f_2$, $f_1 + f_3$ and $f_1 + f_2 + f_3$ (the improved Born approximation) respectively.

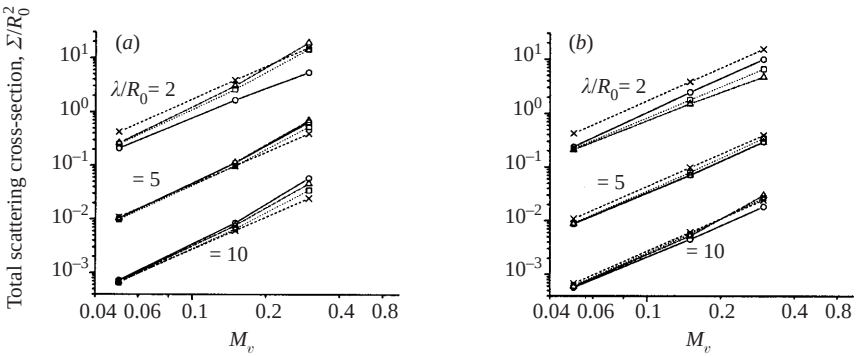

FIGURE 13. Total scattering cross-sections. (*a*) $M_v > 0$, (*b*) $M_v < 0$: ○, DNS; ×, MAE; □, the Born approximation of Kambe & Mya Oo; △, the present Born approximation.

DNS and the present Born approximation except for $|M_v| = 0.15$, 0.3 and $\lambda = 2R_0$. The deviation is rather large for $M_v = -0.3$ and $\lambda = 10R_0$ where the present Born approximation gives too large a value in $90° < \theta < 180°$. It should be noted that the value of Σ differs by a factor of 2–4 for $|M_v| = 0.15, 0.3$ and $\lambda = 2R_0$.

5. Conclusions

Acoustic scattering by HSV and a Gaussian vortex ring has been studied by DNS, and compared with theoretical predictions by MAE and the Born approximation. For long waves with $\lambda/R_0 = 5$, 10, the three predictions are in reasonable agreement with the DNS results when the Mach number is sufficiently small ($|M_v| = 0.05$). For moderate Mach numbers $|M_v| = 0.15$, 0.3, the improved Born approximation gives the best prediction and the difference between DNS and MAE becomes larger. For short waves $\lambda/R_0 = 2$, MAE fails to predict the directivity of the scattered wave correctly. The improved Born approximation is in good agreement with DNS for small Mach number $|M_v| = 0.05$. For moderate Mach numbers $|M_v| = 0.15$, 0.3, however, it fails to give correct magnitudes of the scattered wave while it predicts the directivity correctly.

These results may be understood if we recall the assumptions required for MAE and the Born approximation. MAE requires that the Mach number of the flow be small and the wavelength of the incoming wave be large. On the other hand the Born approximation requires only that the magnitude of the scattered wave be small, though this condition is readily satisfied for large wavelengths as inferred from the MAE result $p_s/|p_i| \propto M\lambda^{-2}$. This is one of the reasons why the Born approximation has a wider range of validity. Another reason is that the Born approximations used in the present study include higher-order effects of Mach number. It should be noted that the Born approximation is much improved by including the Doppler factor $1 - M_v \cos\theta$ and the higher-order terms in the Lighthill tensor. MAE should give better predictions if we include higher-order terms, but this is not an easy task.

The Born approximations are not rational derivations, but the results of this study (see figure 10) show why they are effective approximations in the parameter range examined, and hence verify their validity. This is important to validate their use in other situations.

Finally, we remark on the effect of the problem being three-dimensional on the acoustic scattering by vortices. There are two differences between the present three-dimensional case and two-dimensional scattering by a line vortex. First, in the present case the directivity of the scattering amplitude depends rather weakly on the details of the vortex, namely Mach number and vorticity distribution. As remarked above, the major dependence comes from the Doppler effect. In the case of a line vortex, the directivity depends on the details of the vortex in a more significant way. For example, the number of peaks in the scattering amplitude increases with Mach number (Colonius *et al.* 1994). This feature influences attempts to use scattering data to measure the parameters of compact vortices: we cannot deduce much information from them even when the wavelength is comparable to the size of vortex ($\lambda/R_0 = 2$). Second, as seen in figure 3, the scattering amplitude is inversely proportional to the distance from vortices, as in the case of linear waves generated by a compact source. In the two-dimensional case, when the total circulation of the vortices is not zero, the scattering amplitude does not decay as $r^{-1/2}$, which would be the case for linear waves generated by a two-dimensionally compact source. From an analytical point of view, long-range refraction effects are mainly responsible for these differences. They are strong for line vortices with non-vanishing circulation, but absent for compact vortices.

Y. H. is grateful for the visiting research program by SVBL of Kyushu Institute of Technology. S. G. L. S. acknowledges a UCSD Faculty Career Development Program award. The order of authorship is alphabetical.

Appendix A. Improved Born approximation

We seek an expression for the solution to

$$\frac{1}{c_0^2}\frac{\partial^2 p_s}{\partial t^2} - \nabla^2 p_s = \frac{\partial^2}{\partial x_i \partial x_j}(\rho_{\text{in}} v_i v_j), \tag{A 1}$$

where ρ_{in} is the incoming wave and $\boldsymbol{v}$ is the velocity field of the vortex ring. In the following we proceed as in Kambe & Mya Oo (1981). Since $\rho_{\text{in}} v_i v_j$ decays faster than $|\boldsymbol{x}|$, the solution to (A 1) is given by

$$p_s(t, \boldsymbol{x}) = \frac{1}{4\pi c_0^2}\frac{n_i n_j}{|\boldsymbol{x}|}\frac{\partial^2}{\partial t^2}\int (\rho_{\text{in}} v_i v_j)_{t-r/c_0}\, \mathrm{d}\boldsymbol{y} + O\left(\frac{1}{|\boldsymbol{x}|^2}\right), \tag{A 2}$$

where $\boldsymbol{n} = \boldsymbol{x}/|\boldsymbol{x}|$ and $r = |\boldsymbol{x} - \boldsymbol{y}|$ (Goldstein 1976). We take the incoming wave to be

$$\rho_{\text{in}} = \frac{|p_i|}{c_0^2} \exp[\mathrm{i}(k_0 x_1 - \omega_0 t)] \tag{A 3}$$

and write $B_{ij} = v_i v_j$. By assuming that the size of vortex ring is much smaller than $|\boldsymbol{x}|$ and expanding r as $r = |\boldsymbol{x}| - (\boldsymbol{x} \cdot \boldsymbol{y})/|\boldsymbol{x}| + O(|\boldsymbol{x}|^{-1})$, we have

$$\begin{aligned} p_s(\boldsymbol{x}, t) &= \frac{|p_i|}{4\pi c_0^4} \frac{n_i n_j}{|\boldsymbol{x}|} \frac{\partial^2}{\partial t^2} \int B_{ij}\left(t - \frac{r}{c_0}, \boldsymbol{y}\right) \exp\left(\mathrm{i}\left[k_0 y_1 - \omega_0\left(t - \frac{r}{c_0}\right)\right]\right) \mathrm{d}\boldsymbol{y} \\ &= \frac{|p_i|}{4\pi c_0^4} \frac{n_i n_j}{|\boldsymbol{x}|} \frac{\partial^2}{\partial t^2} \left\{ \exp[-\mathrm{i}(\omega_0 t - k_0|\boldsymbol{x}|)] \int B_{ij}\left(t - \frac{r}{c_0}, \boldsymbol{y}\right) \exp(-\mathrm{i}\boldsymbol{\kappa} \cdot \boldsymbol{y}) \, \mathrm{d}\boldsymbol{y} \right\} \\ &\quad + O\left(\frac{1}{|\boldsymbol{x}|^2}\right), \end{aligned} \tag{A 4}$$

where $\boldsymbol{\kappa} = k_0(\boldsymbol{n} - \boldsymbol{i})$ and $i_l = \delta_{1l}$ is the unit vector in the direction of the incoming wave. Using Fourier transformation, the integral in the above equation becomes

$$\int B_{ij}\left(t - \frac{r}{c_0}, \boldsymbol{y}\right) \exp(-\mathrm{i}\boldsymbol{\kappa} \cdot \boldsymbol{y}) \, \mathrm{d}\boldsymbol{y} = \frac{1}{2\pi} \int \tilde{B}_{ij}(\omega, \boldsymbol{\kappa}_*) \exp\left[\mathrm{i}\omega\left(t - \frac{|\boldsymbol{x}|}{c_0}\right)\right] \mathrm{d}\omega, \tag{A 5}$$

where $\boldsymbol{\kappa}_* = \boldsymbol{\kappa} - (\omega/c_0)\boldsymbol{n}$. Since the vortex ring is steady in the moving frame, we have

$$\tilde{B}_{ij}(\omega, \boldsymbol{\kappa}) = 2\pi \tilde{B}_{ij}(\boldsymbol{\kappa}) \delta(\omega + \boldsymbol{\kappa} \cdot \boldsymbol{U}), \tag{A 6}$$

where

$$\tilde{B}_{ij}(\boldsymbol{\kappa}) = \int B'_{ij}(\boldsymbol{y}) \exp(-\mathrm{i}\boldsymbol{\kappa} \cdot \boldsymbol{y}) \, \mathrm{d}\boldsymbol{y}, \tag{A 7}$$

for $B'_{ij}(\boldsymbol{y}) = B_{ij}(t, \boldsymbol{y} - \boldsymbol{U}t)$. Using $\tilde{B}_{ij}(\boldsymbol{k})$, the integral (A 5) becomes

$$\begin{aligned} &\int B_{ij}\left(t - \frac{r}{c_0}, \boldsymbol{y}\right) \exp(-\mathrm{i}\boldsymbol{\kappa} \cdot \boldsymbol{y}) \, \mathrm{d}\boldsymbol{y} \\ &\qquad = \int \tilde{B}_{ij}(\boldsymbol{\kappa}_*) \delta(\omega + \boldsymbol{\kappa}_* \cdot \boldsymbol{U}) \exp\left[\mathrm{i}\omega\left(t - \frac{|\boldsymbol{x}|}{c_0}\right)\right] \mathrm{d}\omega, \end{aligned} \tag{A 8}$$

$$= \frac{1}{1 - M_n} \tilde{B}_{ij}(\boldsymbol{\kappa}_0) \exp\left[\mathrm{i}\beta\omega_0\left(t - \frac{|\boldsymbol{x}|}{c_0}\right)\right], \tag{A 9}$$

where

$$\boldsymbol{\kappa}_0 = (1 - \beta) k_0 \boldsymbol{n} - k_0 \boldsymbol{i} \tag{A 10}$$

$$\beta = \frac{M_1 - M_n}{1 - M_n}, \quad M_1 = \frac{\boldsymbol{U} \cdot \boldsymbol{i}}{c_0}, \quad M_n = \frac{\boldsymbol{U} \cdot \boldsymbol{n}}{c_0}. \tag{A 11}$$

Finally we obtain

$$p_s = |p_i| \frac{1}{|\boldsymbol{x}|} f(\boldsymbol{n}, \boldsymbol{i}) \exp\left[-\mathrm{i}\omega_s\left(t - \frac{|\boldsymbol{x}|}{c_0}\right)\right], \tag{A 12}$$

where $\omega_s = (1 - \beta)\omega_0$ and

$$f(\boldsymbol{n}, \boldsymbol{i}) = -\frac{\omega_s^2}{4\pi c_0^4} \frac{1}{1 - M_n} n_i n_j \tilde{B}_{ij}(\boldsymbol{\kappa}_0). \tag{A 13}$$

A similar analysis with $\rho_{\text{in}} v_i v_j$ replaced by $\rho_{\text{in}}(c^2 - c_0^2)\delta_{ij}$ gives (3.7).

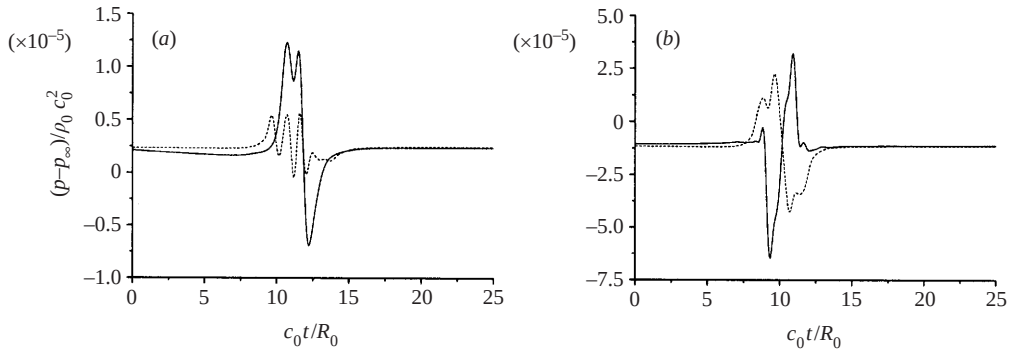

FIGURE 14. Evolution of pressure $p_v - p_0$ for two types of initial conditions: HSV (solid lines) and compressible HSV (broken lines). $M_v = 0.15$, $r/R_0 = 10$. (*a*) $\theta = 0°$, (*b*) $\theta = 90°$.

Appendix B. Initial transient

The initial conditions prepared as we describe in § 4.1 are not steady solutions to the compressible Navier–Stokes equations, which include dissipation and compressibility. As a result, calculations including vortices also contain transient waves. These are emitted at the beginning of the calculation, so we call them initial transients. It is of some interest to see the difference in initial transients between the incompressible HSV and the compressible HSV (figure 14). Initial transients are seen at around $c_0t/R_0 = 10$. The magnitude of initial transients is smaller for the compressible HSV than for the incompressible HSV, while the difference is small for $\theta = 90°$. The reason why using the compressible HSV by LSF*b* instead of the incompressible HSV does not greatly reduce the initial transients is probably that it has an $O(M^2)$ discontinuity in the radial component of velocity at the deformed boundary. We avoid this discontinuity by choosing the boundary between inner and outer solutions for radial velocity so that it is continuous, but this deformation of the boundary is only a compromise as it produces additional vorticity. For all practical purposes, however, subtracting p_v from p_t perfectly removes the initial transients and they do not affect the scattered waves.

REFERENCES

BATCHELOR, G. K. 1956 Wave scattering due to turbulence. In *Symposium on Naval Hydrodynamics*, pp. 409–423. National Academy of Sciences – National Research Council, Washington, DC.

COLONIUS, T., LELE, S. K. & MOIN, P. 1994 The scattering of sound waves by a vortex: numerical simulations and analytical solutions. *J. Fluid Mech.* **260**, 271–298.

CROW, S. C. 1970 Aerodynamic sound emission as a singular perturbation problem. *Stud. Appl. Maths* **49**, 21–44.

DERNONCOURT, B., PINTON, J.-F. & FAUVE, S. 1998 Experimental study of vorticity filaments in a turbulent swirling flow. *Physica* D **117**, 181–190.

FABRIKANT, A. L. 1983 Sound scattering by vortex flows. *Sov. Phys. Acoust.* **29**, 152–155.

FERZIGER, J. H. 1974 Low-frequency acoustic scattering from a trailing vortex. *J. Acoust. Soc. Am.* **56**, 1705–1707.

FETTER, A. L. 1964 Scattering of sound by a classical vortex. *Phys. Rev.* **136**, 1488–1493.

FORD, R. & LLEWELLYN SMITH, S. G. 1999 Scattering of acoustic waves by a vortex. *J. Fluid Mech.* **386**, 305–328.

FUKUMOTO, Y. & MOFFATT, H. K. 2000 Motion and expansion of a viscous vortex ring. Part 1. A higher-order asymptotic formula for the velocity. *J. Fluid Mech.* **417**, 1–45.

Fukuyu, A., Ruzi, T. & Kanai, A. 1994 The response of Hill vortex to a small 3-dimensional disturbance. *J. Phys. Soc. Japan* **63**, 510–527.

Georges, T. M. 1972 Acoustic ray propagation through a model vortex with a viscous core. *J. Acoust. Soc. Am* **51**, 206–209.

Goldstein, M. E. 1976 *Aeroacoustics*. McGraw-Hill.

Golemshtok, G. M. & Fabrikant, A. L. 1980 Scattering and amplification of sound waves by a cylindrical vortex. *Sov. Phys. Acoust.* **26**, 209–213.

Grasso, F. & Pirozzoli, S. 2000 Shock-wave–vortex interactions: shock and vortex deformations, and sound production. *Theor. Comput. Fluid Dyn.* **13**, 421–456.

Hardin, J. C. & Hussaini, M. Y. (Eds.) 1993 *Computational Aeroacoustics*. Springer.

Howe, M. S. 1983 On the scattering of sound by a vortex ring. *J. Sound Vib.* **87**, 567–571.

Howe, M. S. 1984 On the absorption of sound by turbulence and other hydrodynamic flows. *IMA J. Appl. Maths* **32**, 187–209.

Howe, M. S. 1999 On the scattering of sound by a rectilinear vortex. *J. Sound Vib.* **227**, 1003–1017.

Inoue, O. & Hattori, Y. 1999 Sound generation by shock–vortex interactions. *J. Fluid Mech.* **380**, 81–116.

Inoue, O., Hattori, Y. & Sasaki, T. 2000 Sound generation by coaxial collision of two vortex rings. *J. Fluid Mech.* **424**, 327–365.

Kambe, T. & Mya Oo, U. 1981 Scattering of sound by a vortex ring. *J. Phys. Soc. Japan* **50**, 3507–3516.

Kop'ev, V. F. & Leont'ev, E. A. 1987 Radiation and scattering of sound from a vortex ring. *Fluid Dyn.* **22**, 398–409.

Kraichnan, R. H. 1953 The scattering of sound in a turbulent medium. *J. Acoust. Soc. Am.* **25**, 1096–1104.

Labbé, R. & Pinton, J.-F. 1998 Propagation of sound through a turbulent vortex. *Phys. Rev. Lett.* **81**, 1413–1416.

Lele, S. K. 1992 Compact finite difference schemes with spectral-like resolution. *J. Comput. Phys.* **103**, 16–42.

Lighthill, M. J. 1952 On sound generated aerodynamically. I. General theory. *Proc. R. Soc. Lond.* A **211**, 564–587.

Lighthill, M. J. 1953 On the energy scattered from the interaction of turbulence with sound or shock waves. *Proc. Camb. Phil. Soc.* **49**, 531–551.

Lindsay, R. B. 1948 Compressional wave front propagation through a simple vortex. *J. Acoust. Soc. Am.* **46**, 89–94.

Llewellyn Smith, S. G. & Ford, R. 2001*a* Three-dimensional acoustic scattering by vortical flows. Part I: General theory. *Phys. Fluids* **13**, 2876–2889 (referred to herein as LSF*a*).

Llewellyn Smith, S. G. & Ford, R. 2001*b* Three-dimensional acoustic scattering by vortical flows. Part II: Axisymmetric scattering by Hill's spherical vortex. *Phys. Fluids* **13**, 2890–3000 (referred to herein as LSF*b*).

Lund, F. & Rojas, C. 1989 Ultrasound as a probe of turbulence. *Physica* D **37**, 508–514.

Manneville, S., Robres, J. H., Maurel, A., Petitjeans, P. & Fink, M. 1999 Vortex dynamics investigation using an acoustic technique. *Phys. Fluids* **11**, 3380–3389.

Mitchell, B. E., Lele, S. K. & Moin, P. 1995 Direct computation of the sound from a compressible co-rotating vortex pair. *J. Fluid Mech.* **285**, 181–202.

Mitchell, B. E., Lele, S. K. & Moin, P. 1999 Direct computation of the sound generated by vortex pairing in an axisymmetric jet. *J. Fluid Mech.* **383**, 113–142.

Moffatt, H. K. & Moore, D. W. 1978 The response of Hill's spherical vortex to a small axisymmetric disturbance. *J. Fluid Mech.* **87**, 749–760.

Müller, E.-A. & Matschat, K. R. 1959 The scattering of sound by a single vortex and turbulence. *Tech. Rep.* Max-Planck-Institut für Strömungsforschung Göttingen.

Norbury, J. 1973 A family of steady vortex rings. *J. Fluid Mech.* **57**, 417–431.

Obukhov, A. M. 1941 Über die Schallstreuung in der turbulenten Strömung. *Dokl. Akad. Nauk. SSSR* **30**, 616–620.

Oljaca, M., Gu, X., Glezer, A., Baffico, M. & Lund, F. 1998 Ultrasound scattering by a swirling jet. *Phys. Fluids* **10**, 886–898.

O'Shea, S. 1975 Sound scattering by a potential vortex. *J. Sound Vib.* **43**, 109–116.

Pitaevskii, L. P. 1959 Calculation of the phonon part of the mutual friction force in superfluid helium. *Sov. Phys. JETP* **8**, 888–890.

Poinsot, T. J. & Lele, S. K. 1992 Boundary conditions for direct simulations of compressible viscous flows. *J. Comput. Phys.* **101**, 104–129.

Reinschke, J., Möhring, W. & Obermeier, F. 1997 Scattering of sound waves by a cylindrical vortex: a semi-analytical theory. *J. Fluid Mech.* **333**, 273–300.

Saffman, P. G. 1970 The velocity of viscous vortex rings. *Stud. Appl. Maths* **49**, 371–380.

Saffman, P. G. 1992 *Vortex dynamics.* Cambridge University Press.

Sakov, P. V. 1993 Sound scattering by a vortex filament. *Acoust. Phys.* **39**, 280–282.

Sullivan, J. P., Widnall, S. E. & Ezekiel, S. 1973 Study of vortex rings using a laser Doppler velocimeter. *AIAA J.* **11**, 1384–1389.

Tanaka, K. & Ishii, S. 1981 Scattering of a plane sound wave by a vortex pair. *J. Phys. Soc. Japan*, **51**, 1992–1999.

Tang, S. K. & Ko, N. W. M. 1997 Sound generation by interaction of two inviscid two-dimensional vortices. *J. Acoust. Soc. Am.* **102**, 1463–1473.